A mesoscopic model of a two-dimensional solid state structural transformation: statics and dynamics

2004 J. Phys.: Condens. Matter 16 7733

(http://iopscience.iop.org/0953-8984/16/43/013)

INSTITUTE OF PHYSICS PUBLISHING JOURNAL OF PHYSICS: CONDENSED MATTER

J. Phys.: Condens. Matter **16** (2004) 7733–7752 PII: S0953-8984(04)80851-8

A mesoscopic model of a two-dimensional solid state structural transformation: statics and dynamics

Madan Rao[1,2] **and Surajit Sengupta**[3,4]

[1] Raman Research Institute, C V Raman Avenue, Sadashivanagar, Bangalore 560080, India
[2] National Centre for Biological Sciences, UAS-GKVK Campus, Bellary Road, Bangalore 560 065, India
[3] Satyendra Nath Bose National Centre for Basic Sciences, Block J D, Sector III, Salt Lake, Kolkata 700098, India

E-mail: surajit@bose.res.in

Received 15 May 2004, in final form 20 September 2004
Published 15 October 2004
Online at stacks.iop.org/JPhysCM/16/7733
doi:10.1088/0953-8984/16/43/013

Abstract

We study the equilibrium properties of a system of particles in two dimensions, interacting via pair and three-body potentials. This system undergoes a structural transition from a square to a rhombic lattice and thus constitutes a simple model for a generic tetragonal to orthorhombic transition. We aim at an intermediate level of description lying in between that of coarse grained elastic strain Hamiltonians and microscopic *ab initio* approaches. We obtain macroscopic thermodynamic properties and the phase diagram at zero and finite temperatures as a function of the density and the relative strengths of the pair and three-body energies using lattice sums, an approximate 'cell model' theory and molecular dynamics simulations in the NVT ensemble. In addition, we study the dynamics of nucleation following a quench from the square to the triangular phase (Rao and Sengupta 2003 *Phys. Rev. Lett.* **91** 045502). As in real solids, the final microstructure depends sensitively on the depth of the quench—a shallow quench results in an equilibrium *ferrite* while a deep quench gives rise to a metastable twinned *martensite*. We find, in accordance with experiments, that the twinned martensite is associated with a diffusionless transformation. We propose that this model solid may be used as a test bed for studies of the statics and dynamics of structural transitions.

1. Introduction

In spite of its fundamental and technological interest, there is as yet no general theoretical framework for predicting the final microstructure of a solid following changes in temperature

[4] Author to whom any correspondence should be addressed.

or stress across a structural transition [1]. This is in part because most experimental studies have focused on technologically important solids which are far from ideal; thus it has been difficult to isolate generic principles amidst the volume of empirical data [2]. Furthermore, the spatial and temporal resolution of *in situ* experimental probes is limited; this makes it difficult to follow microstructural changes at short scales of length and time. We believe progress can only be made if we (a) identify simple 'model' systems which would serve as an arena for detailed studies on the dynamics of structural transitions in solids and (b) develop 'probes' for studying the dynamics and morphology changes at short scales; in other words for *following the motion of individual atoms as the transformation proceeds*. High speed computational modelling allows one to make useful contributions to both (a) and (b). This paper mainly concerns point (a)—we provide a model system for a simple structural transition which could serve as a test bed for studies of statics and dynamics of structural transitions. We demonstrate its usefulness by evaluating the equilibrium phase diagram and computing thermodynamic quantities as functions of temperature and potential parameters. In addition, we have carried out an exhaustive analysis of the dynamics of solid state transformations in this model system (point (b))—here we provide a short description for completeness; a detailed treatment appears in [3]. A unique feature of our analysis is the simultaneous tracking of individual particles at short scales and coarse grained elastic variables at longer scales, *as the transformation proceeds*.

Our choice of the simple structural transformation, a square to a rhombic lattice in two dimensions (2D), is motivated by two important considerations. The first is its relevance to 'real' solid state transformations. The square to rhombus transition may be regarded as a rather accurate representation [4] of the three-dimensional tetragonal to orthorhombic (TO) transition in an oriented single crystal where the strain along the third direction (c-axis) is negligible. This transition is observed in many technologically important systems [5], such as the high T_c compound $YBa_2Cu_3O_7$. A novel realization of such a structural transformation occurs in charged textures in $\nu = 1$ quantum Hall systems [6].

The second motivation is more conceptual and warrants some explanation. Following a quench across a structural transition, the atoms constituting the solid have to rearrange themselves, since the parent phase is thermodynamically unstable. Instead of moving to the new equilibrium configuration, the motion of the atoms is arrested in a final microstructure which is very far from equilibrium. The microstructures often display features at length scales ranging from 1000 Å to 100 μm, many orders larger than the lattice spacing. A more appropriate description of the dynamics at these scales is in terms of continuum degrees of freedom. It is however not clear *a priori* what the relevant continuum degrees of freedom are, especially in situations where the solid undergoes large deformations from the parent. In most theoretical studies of this problem, the only continuum degrees of freedom relevant at these scales have been taken to be the components of the strain tensor [4, 7]. However, short length scale phenomena such as atomic rearrangements [3, 8, 9] are not captured by these strain-only theories and may in some cases affect the kinetics of the transformation. The only unbiased way to determine the complete set of relevant degrees of freedom in the continuum is to start from a more microscopic description and arrive at a continuum description using a coarse graining method [10]. Such a coarse graining programme is more easily set up in the crystallographically simpler square to rhombus transition.

How microscopically detailed should our microscopic model solid be? An *ab initio* or semi-empirical description [11] which includes electronic degrees of freedom tailor-made for a real system such as $YBa_2Cu_3O_7$ suffers from three drawbacks—(i) it compromises the need for generality, (ii) it is computationally expensive and (iii) it is difficult to extrapolate to the continuum. We therefore model an *effective* Hamiltonian accurate over distances smaller than

the bulk elastic correlation length but larger than the typical atomic spacing. This effective Hamiltonian, coarse grained over the faster electronic degrees of freedom, will in general have pair and many-body interactions. Note that in as much as the effective interactions are not the microscopic, bare interactions, the 'effective atoms' are not the microscopic, bare atoms.

Our model system therefore consists of a set of N 'particles' confined in a 2D box of volume V at a fixed temperature T. The particles interact with each other via specific two- and three-body [12] interactions. While the two-body interaction stabilizes a rhombic lattice (triangular for *isotropic* two-body potentials), the three-body interactions have been *constructed* to favour a square lattice. Unlike in a real solid, the square to triangular transition in our model solid may be driven by *independently* (i) increasing the density, (ii) decreasing the temperature or (iii) decreasing the relative magnitude of the three-body potential. We discuss, in the main, the equilibrium aspects of this transition. Towards the end, we present some results concerning the dynamics of this transition; a detailed account of the dynamics of nucleation and growth is published elsewhere [3]. In the next section we introduce our model, describing the pair and three-body potentials. In section 3 we present the static lattice (zero-temperature) results for the energy, stress and the elastic constants and exhibit the zero-temperature phase diagram. In section 4 we discuss the effect of finite temperatures. We present results both from a 'cell model' approximation [13, 14] and from molecular dynamics simulations [15] in the NVT ensemble. In section 5 we discuss a simple generalization of the model to include a molecular solid with a complex basis motif. We discuss briefly the dynamics of solid state nucleation following a quench across the structural transition in section 6. Section 7 presents a conclusion and future directions of this work.

2. The model potential

In this section we motivate the form of the *effective* Hamiltonian, coarse grained over the faster electronic degrees of freedom. Instead of starting out *ab initio*, we shall assume that the solid can be described by a general functional of the densities of particles. A simple form of the density functional, proposed by Ramakrishnan and Yussouff (RY) [18], views the solid as an extremely inhomogeneous liquid with a non-uniform, periodic, coarse grained density $\rho(\mathbf{r})$. The advantage of this approach is that it allows us to make accurate statements at any finite temperature $k_{\mathrm{B}}T = \beta^{-1}$. Following RY, we may write the Helmholtz free energy F_{s} per unit volume V of the solid as

$$\frac{\beta F_{\mathrm{s}}}{V} = \frac{1}{v}\int_v \mathrm{d}^3 r[\rho(\mathbf{r})\ln(\rho(\mathbf{r})/\rho_{\mathrm{s}}) - \rho_{\mathrm{s}}] - \frac{1}{2}\sum_{\mathbf{G}} \rho_{\mathbf{G}}\rho_{-\mathbf{G}}C^{(2)}(\mathbf{G}) - \tfrac{1}{3}\sum_{\mathbf{G}_1,\mathbf{G}_2} \rho_{\mathbf{G}_1}\rho_{\mathbf{G}_2}\rho_{-\mathbf{G}_1-\mathbf{G}_2}C^{(3)}(\mathbf{G}_1,\mathbf{G}_2,-\mathbf{G}_1-\mathbf{G}_2) + \cdots. \tag{1}$$

The leading term gives the ideal gas contribution (the integral is over the Wigner–Seitz unit cell of volume v), while the subsequent terms arise from the interactions between density waves $\rho_{\mathbf{G}}$ with wavevector $\mathbf{G}$ belonging to the set $\{\mathbf{G}\}$ of reciprocal lattice vectors (RLV) of the crystalline solid. Note that we have defined the Fourier transform as

$$\rho_{\mathbf{G}} = \frac{1}{v}\int_v \mathrm{d}^3 r\, \mathrm{e}^{\mathrm{i}\mathbf{G}\cdot\mathbf{r}}\rho(\mathbf{r}). \tag{2}$$

The interaction terms involve the Fourier transform of the nth-order direct correlation functions $C^{(n)}(\mathbf{G}_1,\mathbf{G}_2,\ldots,\mathbf{G}_{n-1})$. These functions may either be evaluated from a liquid state theory [19] or deduced from scattering experiments (for instance, $C^{(2)}(q) = 1 - \rho_{q=0}/S(q)$, where $S(q)$ is the structure factor of the liquid at wavenumber q); however, evaluation

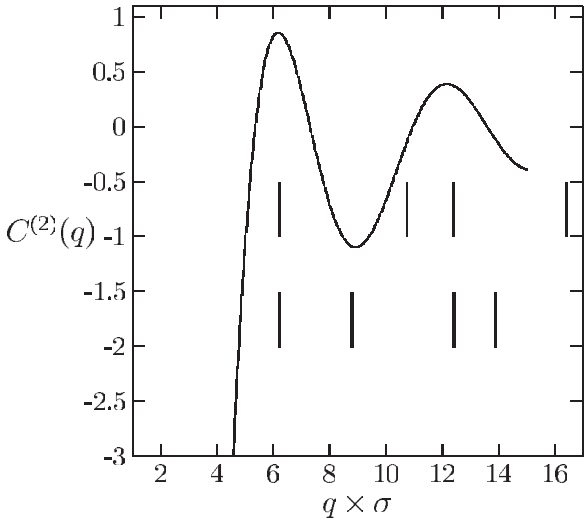

Figure 1. A plot of the second-order direct correlation function $C^{(2)}(q)$ versus wavenumber q for a supercooled hard disc liquid in two dimensions. The lines mark the lengths of the reciprocal lattice vectors for the triangular (top) and the square (bottom) lattices scaled so that the smallest RLV corresponds to the first peak in $C^{(2)}(q)$.

(or measurement) of direct correlation functions beyond the second order is extremely difficult [20]. Approximate ways of incorporating the effects of these higher order correlations have been used with varying degrees of success [21], though often a simple weak coupling (mean-field) approximation, $C^{(n)} = V^{(n)}/k_{\mathrm{B}}T$, where $V^{(n)}$ is the n-body potential, works remarkably well [22].

While the ideal gas term always favours a uniform liquid, the sign of the interaction term decides whether the interactions stabilize (destabilize) density waves with wavevectors $\mathbf{G} \neq 0$. As an example, let us consider first the effect of only the second-order terms in equation (1). The coefficients, $C^{(2)}(|\mathbf{G}|)$, measure the stability of a density wave with wavenumber $|\mathbf{G}|$. In figure 1 we have plotted $C^{(2)}(q)$ against q for a slightly supercooled hard disc liquid [23] in two dimensions. This function is oscillatory and has a primary peak at roughly the wavenumber corresponding to the magnitude of the smallest RLV of the thermodynamically stable solid. Choosing the lattice parameter such that the smallest RLV coincides with the first peak of $C^{(2)}(q)$, we have plotted the positions of the RLVs for the triangular (top) and square (bottom) lattices in figure 1. Close-packed lattices have RLVs which are, on average, more widely separated than those of an open lattice. As a consequence, open lattices often have RLVs lying in the region of the first *minimum* of $C^{(2)}(q)$ which is negative, thereby contributing to a destabilization of the lattice. From figure 1 we observe that this is indeed the case for the square lattice in two dimensions [24]. Density waves corresponding to the second RLV of the square lattice with Miller index {11} are not favoured, making the square lattice unstable in two dimensions.

Note that the discussion above is the finite T generalization of the zero-temperature result: that for isotropic, purely repulsive *pair* potentials in two dimensions, one can only stabilize the close-packed triangular lattice [16]. For instance, a static calculation [17] of the $T = 0$ elastic moduli of the square lattice reveals a shear instability which spontaneously distorts the lattice until it regains a close-packed structure.

In order to stabilize the square lattice one needs to go beyond the second-order contribution and consider the effect of three-body correlations. As is clear from equation (1), a positive (and large enough!) contribution from $C^{(3)}(\mathbf{G}_1, \mathbf{G}_2, -\mathbf{G}_1 - \mathbf{G}_2)\rho(\mathbf{G}_1)\rho(\mathbf{G}_2)\rho(-\mathbf{G}_1 - \mathbf{G}_2)$, where any one (or two) of the wavevectors equals {11}, can compensate for the destabilizing effect of the second-order correlator [24]. There are many choices for the wavevectors $\mathbf{G}$, but

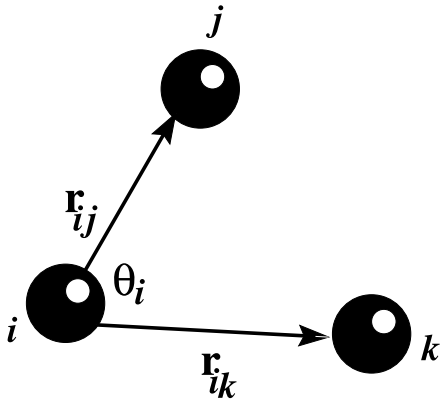

Figure 2. Definition of angles and distances used in the three-body potential.

the simplest combination is $\mathbf{G}_1 = \mathbf{G}_2 = \{10\}$ (so that $\{10\} + \{01\} = \{11\}$). A straightforward way to ensure that this combination of density waves is stabilized is to stabilize the *real space* triangle involving the direct lattice vectors (10), (01) and (11) (and those related to them by symmetry). Within a simple minded mean-field approximation this may be accomplished, as shown below, by choosing an appropriate three-body potential which favours 0°, 45° and 90° bonds. Higher order interactions involving four or more particles, though present in principle, are not necessary for our purpose.

Our model system, constructed from this level of coarse graining, therefore consists of 'point particles' interacting with effective pair and three-body potentials. The interaction energy E of the system is given by

$$E = \tfrac{1}{2}\sum_{i\neq j}\Psi_2(\mathbf{r}_{ij}) + \tfrac{1}{6}\sum_{i\neq j\neq k}\Psi_3(\mathbf{r}_{ij},\mathbf{r}_{jk},\mathbf{r}_{ki}). \tag{3}$$

For the pair potential we take

$$\Psi_2(|\mathbf{r}_{ij}|) = V_2\left(\frac{\sigma}{|\mathbf{r}_{ij}|}\right)^{12}, \tag{4}$$

which is purely repulsive and therefore the system has to be confined with a uniform hydrostatic pressure (see below). A purely repulsive system simplifies our analysis since there is one fewer length scale and one fewer non-solid phase. Without the three-body potential, our system is characterized by only one parameter instead of two (temperature and density). On including the three-body potential, we lose this simplification, but the variation of thermodynamic properties with density is still weak. Without loss of generality we can take V_2 and σ to be our units for energy and distance respectively.

The three-body potential is

$$\Psi_3(\mathbf{r}_{ij},\mathbf{r}_{jk},\mathbf{r}_{ki}) = V_3\Big[f_{ij}\sin^2(4\Theta_i)f_{ik} + f_{ij}\sin^2(4\Theta_j)f_{jk} + f_{jk}\sin^2(4\Theta_k)f_{ki}\Big] \tag{5}$$

where the function

$$f_{ij} \equiv f(r_{ij}) = \begin{cases} (r_{ij}-r_0)^2 & r_{ij} < r_0, \\ 0 & \text{otherwise}, \end{cases} \tag{6}$$

and we have used the notation $r_{ij} \equiv |\mathbf{r}_{ij}|$. The angles are as defined in figure 2. The function f_{ij} provides a cut-off for the three-body potential; as long as f_{ij} is short ranged (we have taken $r_0 = 1.8\sigma$), the actual form of this function does not affect the qualitative results.

Note the close resemblance to the Weber–Stillinger potential [12]; our model however has stronger square correlations built in, making the resulting structural transition (see below)

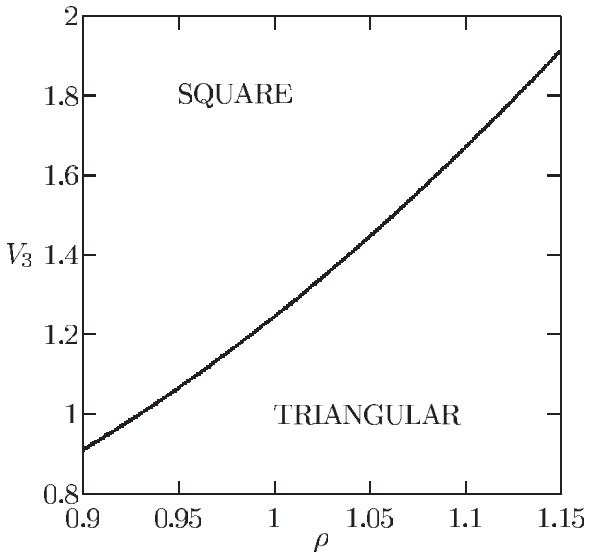

Figure 3. The zero-temperature phase diagram in the V_3–ρ plane. The regions where the square and the triangular phases are stable are labelled.

strongly first order. Moreover, while Weber and Stillinger concentrate on the equilibrium solid to liquid transition, we use this model to study the statics and dynamics of solid–solid transformations in great detail.

It may appear that a three-body potential requires a large investment in terms of computer times. This apprehension is fortunately unfounded. The form of this potential ensures that three-body energies can be calculated [12] extremely efficiently, requiring a computational effort not exceeding that for the pair part. This is discussed in the appendix.

3. Zero temperature: equilibrium

At zero temperature, the equilibrium configuration is a solid which minimizes the potential E. Since we work in the constant NVT (and shape) ensemble, the density $\rho = N/V$ is a constant. Assuming that the only minima of E correspond to the triangular or square phases, we have numerically deduced the $T = 0$ phase diagram in the ρ–V_3 plane (figure 3). Later in this section we show, within a restricted variational calculation, that these are the only minimizers of E. As we see from figure 3, the triangular lattice is the lowest energy phase at high densities and small values of V_3, i.e., wherever the pair interaction dominates over the three-body part. Across the boundary there is a strong first-order transition with a discontinuous change in the slope $(\partial E/\partial\rho)_{V_3}$.

To deduce the nature of the order parameter distinguishing the square from the triangular phase, we look at how a rhombic lattice may be obtained from a square. Such an analysis makes contact with continuum elasticity in a natural way.

At zero temperature, a continuous family of perfect rhombic lattices (labelled by position vectors $\mathbf{R}^{\mathrm{T}}$) can be obtained from the perfect square lattice (labelled by $\mathbf{R}^0$) by the transformation $\mathbf{R}^{\mathrm{T}} = (\mathsf{I} + \mathsf{T})\mathbf{R}^0$ where the transformation matrix T is

$$\mathsf{T} = \begin{pmatrix} \epsilon_1/2 + \epsilon_2/2 & \epsilon_3 \\ \epsilon_3 & \epsilon_1/2 - \epsilon_2/2 \end{pmatrix}. \tag{7}$$

The parameters ϵ_α ($\alpha = 1, 2, 3$) are related to the components of a strain tensor by the following construction. We choose to measure all distortions and energies with respect to the

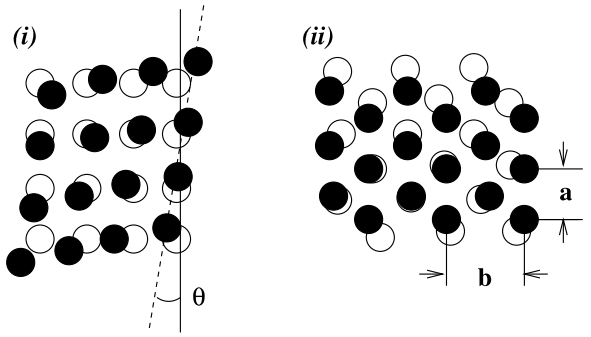

Figure 4. Two equivalent ways of obtaining a triangular lattice (filled circles) from a square, (i) and (ii). One can either (i) shear the original lattice by an angle θ or (ii) rotate the original lattice by 45° and then stretch it along one of the axes and compress it along the other so that $b/a > 1$. For a square lattice, $\theta = 0$, $b/a = 1$ and $\theta = 15°$, $b/a = \sqrt{3}$ for the ideal triangular lattice. In terms of the shear strain ϵ_3 the corresponding numbers are 0 and 0.278 12.

undistorted *square* phase—our reference state. The microscopic displacements $\mathbf{u}_{\mathbf{R}^0} = \mathbf{R}^{\mathrm{T}} - \mathbf{R}^0$ are therefore defined at every $\mathbf{R}^0$ on the reference lattice, i.e., we use *Lagrangian* [16, 25] coordinates. The full nonlinear Lagrangian strain tensor [25] ϵ_{ij} is

$$\epsilon_{ij} = \frac{1}{2}\left(\frac{\partial u_i}{\partial r_j} + \frac{\partial u_j}{\partial r_i} + \frac{\partial u_k}{\partial r_i}\frac{\partial u_k}{\partial r_j}\right), \tag{8}$$

where the indices i, j go over x and y. The parameters ϵ_α in equation (7) represent the combinations $\epsilon_{xx} + \epsilon_{yy}$, $\epsilon_{xx} - \epsilon_{yy}$ and ϵ_{xy} respectively, which reduce to the usual volumetric, deviatoric and shear strains once nonlinearities are neglected. Note that one may start with a prescribed square and end with a final triangular lattice in more than one way—the transformation parameters are not unique. For instance, for a given orientation of the parent square lattice shown in figure 4 (i) one obtains a rhombic lattice using $\epsilon_2 = 0$ and $\tan\theta = \epsilon_3/(1+\epsilon_1)$. Equivalently (figure 4 (ii)) the square lattice (first rotated by 45°) can be transformed to a centred rectangular lattice with $\epsilon_3 = 0$ and $b/a = (1+\epsilon_2+\epsilon_1/2)/(1-\epsilon_2+\epsilon_1/2)$. The two transformations are completely equivalent.

One of the offshoots of this non-uniqueness is that any rhombus obtained as a uniform deformation of a perfect square can be represented by two independent parameters ϵ_1 and ϵ_3. In addition, since the density ρ is a constant in our NVT ensemble, ϵ_1 is related to ϵ_3; $\epsilon_1 = \sqrt{1+\epsilon_3^2} - 1 \approx \epsilon_3^2/2$. Thus all rhombic lattices considered by us can be labelled by a single parameter $\epsilon_3 = \epsilon$ (which by definition is 0 for the perfect square lattice). This makes the shear strain ϵ a good order parameter which distinguishes the square from the triangular lattices.

We may now calculate the energy of $T = 0$ configurations as a function of the order parameter ϵ. A calculation of the energy E and its derivatives (elastic moduli) for a given lattice involves computation of lattice sums. We start with a finite square lattice containing 10×10 sites and allow the transformation T to produce a continuous sequence of rhombic lattices labelled by ϵ. We have checked for convergence of the lattice sums by increasing the size of the lattice and observing the consequent change in the numerical values. In figure 5 we have plotted the energy per particle E/N as a function of the parameter ϵ for various values of V_3 (keeping ρ fixed). Note that for large values of V_3 there is only one minimum at $\epsilon = 0$, so the square lattice is the only stable phase. For smaller values of V_3 two additional degenerate minima appear at $\epsilon = \pm\epsilon_0 = \pm 0.278\,12$ which correspond to the triangular lattice. The

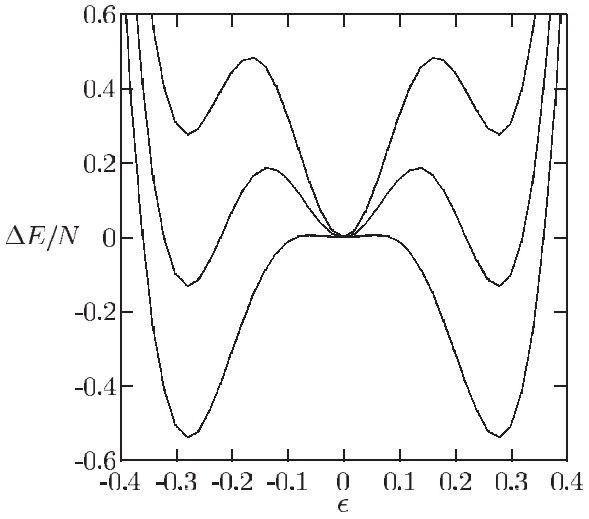

Figure 5. Energy difference per particle ($\Delta E/N$) between the square and rhombic lattices as a function of the strain order parameter ϵ (see the text). Of the three minima shown, the one at $\epsilon = 0$ corresponds to the square phase and the two degenerate minima at $\epsilon = \pm\epsilon_0$ corresponds to two different orientations of the triangular phase. The curves are for $V_3 = 2.0$ (top), 1.5 and 1.0. Note the first-order transition from the square to the triangular phase as V_3 is reduced.

transition is first order with the order parameter jumping discontinuously, $|\Delta\epsilon| = \epsilon_0$. Note that in this model the change in the shear strain across the transition is fixed; we shall return to this point in section 5 where we propose a variant of this model in which the jump in the shear strain across the structural transition can be made arbitrarily small. As expected, the square and triangular lattices are the only minimizers of E within this parametrization scheme.

To make contact with elasticity theory we may compute stresses and elastic moduli, obtained by evaluating appropriate derivatives of the energy keeping T, N, V constant, namely $\partial E/\partial\epsilon_\alpha = \sigma_\alpha$ (figure 6) and $\partial^2 E/\partial\epsilon_\alpha\partial\epsilon_\beta = C_{\alpha\beta}$ (figure 7). Note that our system is always under a hydrostatic pressure $P = \sigma_1$; the constant density constraint implies that for $\epsilon \neq 0$ there is an applied shear stress $\sigma_3 = P(\epsilon)\epsilon$ (figure 6). This implies that the slope of the shear stress versus ϵ_3 curve is not the shear modulus C_{33} (defined for zero external stress) but $C_{33} + P$ (figure 7).

At this stage, we find it useful to point out that the results of figures 5–7 can be rationalized using a systematic power series expansion of the energy in terms of ϵ_α. Although such expansions are quite common in the literature [4, 7], our results show that fourth-order terms in ϵ_α, especially cross-couplings of the form $\epsilon_1^2\epsilon_3^2$ and $\epsilon_2^2\epsilon_3^2$, together with coupling to the external hydrostatic pressure P need to be included in order to reproduce the $T = 0$ results accurately. The coefficients of all these terms are however not independent. For instance, relationships such as

$$\left.\frac{\partial^2 F}{\partial\epsilon_2^2}\right|_{\epsilon_0} = \left.\frac{\partial^2 F}{\partial\epsilon_3^2}\right|_{\epsilon_0} \tag{9}$$

dictated by the geometry of the triangular phase have to be satisfied for all temperatures and densities.

In this section we have been able to show that our model potential indeed produces the square and the triangular lattices as minima of the energy. The potential parameters may be tuned, if necessary, to a real system by comparing the elastic properties of this model system to

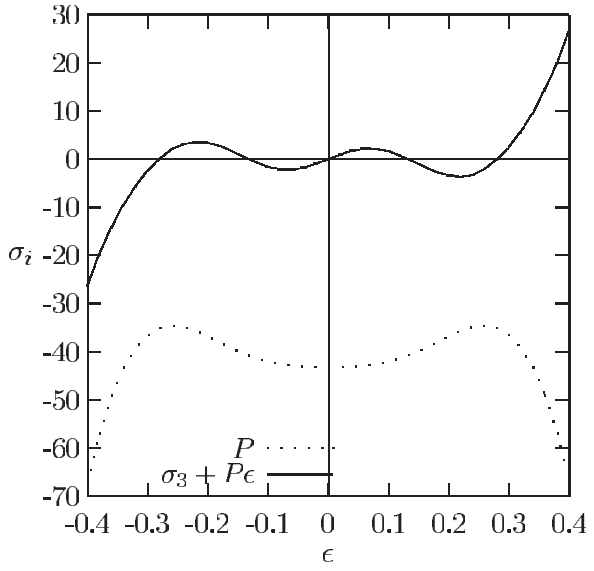

Figure 6. The pressure $P = \sigma_1$ and the 'effective' shear stress $\partial E/\partial\epsilon = \sigma_3 + P\epsilon$ as a function of ϵ for $\rho = 1.1$ and $V_3 = 1.5$.

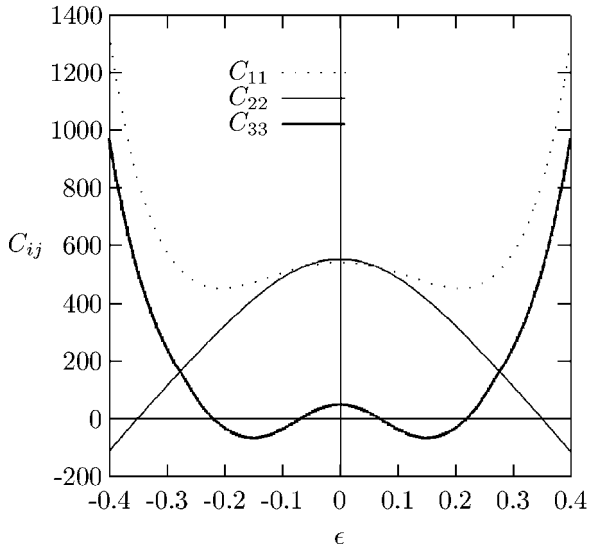

Figure 7. The second-order elastic moduli C_{11} (bulk), C_{22} and $C_{33} + P$ (shear) as a function of ϵ. Note that for the triangular lattice, $C_{22} = C_{33} + P$ as required by symmetry. The density $\rho = 1.1$ and $V_3 = 1.5$.

experimentally measured quantities. By varying the density or the strength of the three-body potential one obtains a zero-temperature first-order structural transition between a square and triangular lattice. What happens to the structural transition at non-zero temperatures? We study this question in the next section.

4. Non-zero temperature: equilibrium

In this section we analyse the phase diagram at $T \neq 0$ as a function of V_3 or ρ. We do this by two methods—an 'exact' molecular dynamics (MD) simulation [15] in the constant NVT ensemble, using the two- and three-body potentials defined earlier, and an approximate 'cell model' [13] based on the deformation parameter ϵ. The latter leads naturally to an approximate

continuum elasticity description at $T \neq 0$. We take up the cell model analysis first and compare its results with the exact MD simulation in the next subsection.

4.1. Cell model approximation: free energies and phase stability

Imagine being in a region of the zero-temperature parameter space V_3–ρ, where the square solid is the stable minimum of the energy. As the temperature is gradually increased, the contribution of the phonon entropy to the (Helmholtz) free energy destabilizes the square lattice. In order to quantify this effect one needs to go beyond the static lattice and consider phonon fluctuations. Although a direct calculation of the contribution of phonons to the lattice energy is straightforward [17], we choose to use the much simpler, though not necessarily less accurate 'cell model' approximation.

Before discussing the cell model approximation, let us mark its regime of validity. First, the cell model approximation neglects contributions from topological defects such as dislocation–antidislocation pairs and thus breaks down near the melting point [10]. In two dimensions, there is a further complication, since fluctuations of the displacement field **u** due to phonons diverge logarithmically [16] with system size. This divergence is however weak and may be ignored for the system sizes under consideration.

Recall that at $T = 0$, the configurations of the perfect rhombi were parametrized by a single deformation variable ϵ. Is this true at $T \neq 0$, when the lattices are not perfect due to phonon vibrations? At low temperatures, we may assume that fluctuations of the rhombic cells are slight—one may therefore be allowed a mean-field decoupling wherein products of the components of strain are replaced by products of the corresponding averages. Arguing as before, the rhombic cells can now be parametrized by $\langle\epsilon_1\rangle$ and $\langle\epsilon_3\rangle$, which in addition are related to each other by the constancy of ρ. Within the spirit of the mean-field approach, we ignore spatial fluctuations of the order parameter, an act justified when the temperatures are low. Thus the energy E may be written as a functional of a spatially independent $\langle\epsilon\rangle$.

Within the cell model approximation, the partition function of a lattice of N particles at temperature T is given by [13]

$$Z(\langle\epsilon\rangle, T, N) = \left[\Lambda^{-3}\int_{v_\epsilon} \mathrm{d}\mathbf{r}\, \exp(-\delta\phi_\epsilon(\mathbf{r})/k_\mathrm{B}T)\right]^N \times \exp(-E(\langle\epsilon\rangle)/k_\mathrm{B}T) \tag{10}$$

where Λ is the thermal wavelength and $\delta\phi$ is the change in potential energy of a single particle as it moves around within a unit cell of size v_ϵ in a potential well arising from its interaction with all its neighbours. A further harmonic approximation for $\delta\phi$ leads to the familiar Einstein approximation. At the other extreme, for the hard disc potential, $\delta\phi = 0$ except where overlaps occur and the cell model approximation becomes identical to the *free volume* [14] theory. The Helmholtz free energy for any rhombic lattice labelled by $\langle\epsilon\rangle$ may now be obtained by using $F = -k_\mathrm{B}T \log Z$.

Evaluation of the Helmholtz free energy (figure 8) allows us to calculate the V_3–T phase diagram at any density ρ, as also the limits of metastability of the square lattice.

4.2. Molecular dynamics simulations

To obtain accurate results for the phase stability at non-zero temperatures, we have performed a molecular dynamics simulation (Newton's laws!) on our model system. We simulate $N = 2499$ particles (50×50 unit cells with a vacancy to improve the kinetics) in the NVT ensemble using a standard Nosé–Hoover thermostat [15]. The equations of motion for the

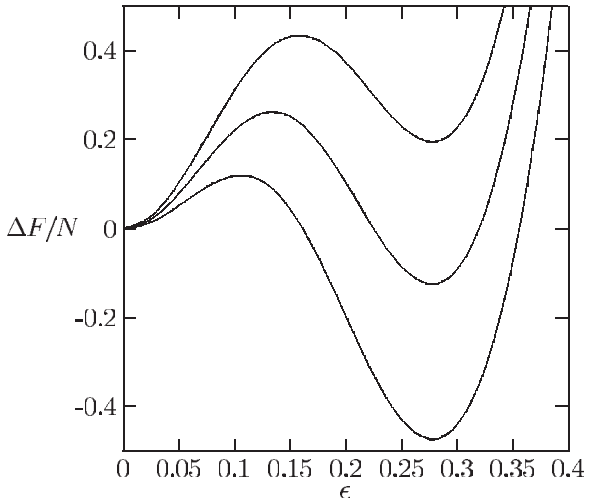

Figure 8. The per particle Helmholtz free energy difference ($\Delta F/N$) between the square ($\langle\epsilon\rangle = 0$) and rhombic lattices as a function of $\langle\epsilon\rangle$ for various temperatures $T = 0.1$ (top), 0.5 and 1 (bottom). Note the first-order phase transition from square to triangular with increasing temperature.

particles coupled to the thermostat are given by [15]

$$\begin{aligned} \frac{\mathrm{d}\mathbf{x}_i}{\mathrm{d}t} &= \frac{\mathbf{p}_i}{m} \\ \frac{\mathrm{d}\mathbf{p}_i}{\mathrm{d}t} &= \mathbf{F}_i - \xi\mathbf{p}_i, \\ \frac{\mathrm{d}\xi}{\mathrm{d}t} &= \frac{2N-3}{Q}(T_{\mathrm{kin}} - T), \end{aligned} \tag{11}$$

where $\mathbf{x}_i$ and $\mathbf{p}_i$ are the positions and momenta of the ith particle respectively and the mass m has been taken to be unity. $\mathbf{F}_i$ is the total force acting on the ith particle due to all other particles and is derivable from the two- and three-body model potentials. The coupling to the heat bath is parametrized by the variable ξ which acts as a force maintaining the kinetic temperature $T_{\mathrm{kin}} = (1/N)\sum_i p_i^2/2m$ at the temperature T of the bath (we have chosen a value of $Q = 0.1$ to ensure convergence).

Note that we use a single (mobile) vacancy in the 50×50 lattice, as a *device* for attaining rapid equilibration. Further, note that the particles move according to Newton's laws, while the vacancy mobility is an ineluctable *consequence* of this particle motion.

Starting from an ideal square lattice, we have equilibrated systems at various values of V_3 and temperature at a fixed density for a time equal to 50–$100 \times \tau$ (where $\tau = \sigma/\sqrt{V_2}$, assuming a unit particle mass—this corresponds to a real time of 1 ps) or until thermodynamic quantities such as the pressure and energy have stabilized. To ensure that the temperature remains fixed to within 1 part in 10^5, we have integrated the equations of motion using a leapfrog algorithm with a time step of $10^{-3}\tau$. The final structure is then examined and the information is used to obtain the phase diagrams shown in figure 9. We display the phase diagram for two densities $\rho = 1.05$ and 1.1. We have also plotted, together with the molecular dynamics results, the results from the cell model approximation. We observe that for low temperatures, the cell model approximation faithfully reproduces the actual phase boundary while showing marked deviations at higher temperatures. The cell model approximation is also used to plot the limit of stability of the square phase in the triangular region.

Both the molecular dynamics simulations and the cell model calculations predict that the square to triangular transition remains first order over a wide region of parameter space even at non-zero temperatures. For larger density, the transition point shifts to higher values of V_3.

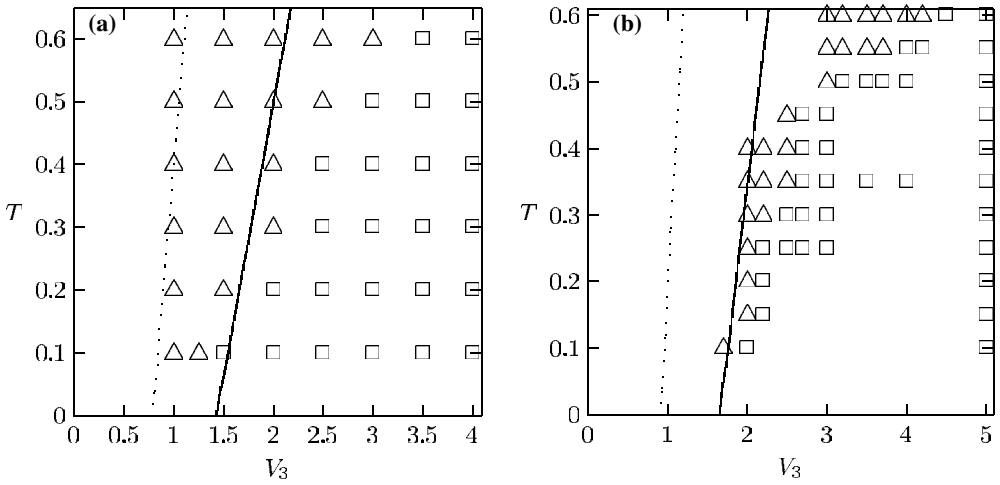

Figure 9. The phase diagram in the T–V_3 plane for $\rho = 1.05$ (a) and 1.1 (b). For large V_3 the square phase is stable while the triangular phase is stable for smaller values of V_3. The points are results from our molecular dynamics simulations in the NVT ensemble with 2499 particles. Starting from an initial ideal square lattice the system was equilibrated for up to 60 000 steps and the final structure noted (□ for square and Δ for triangular) for various values of T and V_3. The solid line is the phase boundary resulting from the cell model approximation (see the text) and the dashed line is the metastability limit for the square phase from the same theory.

This is expected since a high density favours the triangular lattice. Also, the square phase becomes unstable for lower values of V_3 as the density is increased. The jump in the order parameter remains fixed at $|\Delta\epsilon| = \epsilon_0$ along the whole transition line. This aspect of our model is specifically addressed in the next section, where we show that inclusion of an anisotropic *pair* interaction allows one to tune the order parameter jump all the way to zero.

We end this section with the following observations. We have seen that the exact MD and approximate cell model give qualitatively similar results. More sophisticated phonon fluctuation calculations may even produce quantitative agreement. Figure 8 suggests that the Helmholtz free energy may be expanded in powers of $\langle\epsilon\rangle$, just as was noted at $T = 0$. Although we do not explicitly demonstrate it here, we may recover elasticity theory (including corrections arising from thermal fluctuations) by constructively coarse graining as in [10]. Finally we must comment on the effect of finite size on the results of our simulations. In the phase transition, being strongly first order, we do not see any change in the phase boundaries when the number of particles is varied from 50×50 to up to 110×100. The non-equilibrium, intermediate, microstructures do however depend on the size of the system. For example, in order to observe the twinned state as discussed in section 6, one needs a sufficiently large system so that the twin has enough space to grow before it impinges on itself due to periodic boundary conditions.

5. Generalization to molecular solids

The model 2D solid discussed in the preceding sections has the virtue that it is simple enough to begin a detailed theoretical study on, as regards both the equilibrium and dynamical features of the TO transition across a range of scales of length and time. However, if we were to compare the results of such a study with experiments on real systems, we would immediately face a problem. Most solids undergoing a TO transition [4], for instance $YBa_2Cu_3O_7$, have a complex

basis, consisting of many atoms per unit cell. These systems generically have much smaller jumps in the shear strain at the TO transition compared to the jump computed in the previous section. To appreciate the *quantitative* discrepancy, recall the discussion following equation (8), where we showed that any perfect rhombus obtained as a deformation of a square may be parametrized by either ϵ or b/a. Defining an *orthorhombic distortion* as $D \equiv (b-a)/(b+a)$, we find that $D = (\sqrt{3}-1)/(\sqrt{3}+1) \approx 0.27$ for our model square to triangle structural transition—significantly larger than $D = 0.0085$ for the TO transition in $YBa_2Cu_3O_7$.

Apart from this, there might be a more serious *qualitative* mismatch between our model solid and real systems undergoing a TO transition. Changes in temperature or pressure (hydrostatic or chemical) may lead to a local structural rearrangement (optical modes) which would couple to the strain tensor. The jump in the shear strain across the structural transition may therefore, unlike in our model solid, vary along the phase boundary, even going to zero (phonon softening) at a critical point [26].

We shall see that we may address both of these issues within an anisotropic variant of our model solid. Our attempt will be to incorporate the complex basis, with many atoms per unit cell, into an *effective* Hamiltonian between 'point particles'. In the spirit of an effective Hamiltonian, we will coarse grain the density over a scale of length and time corresponding to the 'size' ξ and relaxation time τ of the basis. Thus we may define a coarse grained density as $\rho(\mathbf{r}) = p^{-1}\sum_\mu \rho_\mu(\mathbf{r})$, where $\mu = 1, \ldots, p$ labels the atomic species making up the basis. This coarse grained density profile $\rho(\mathbf{r})$ will have peaks at the centre of mass of each basis, falling off to zero over a length scale ξ and having a cross section which is spatially anisotropic. If we assume that this anisotropic cross section has a fixed shape at a given temperature and pressure (true when the associated optical branch is much higher than the acoustic branches), then we may write the effective Hamiltonian as arising from a collection of 'point particles' interacting via an anisotropic potential. Once again the notion of a 'particle' here is an effective one, coarse grained over the length scale ξ. The form of the effective Hamiltonian may be motivated in terms of a density wave picture [27] in much the same way as in section 2. An anisotropic density interacts via an anisotropic direct correlation function. Within a mean-field approach this reduces to a pair potential which depends not only on the distance between the two basis motifs but also on their orientation relative to the crystal axes—orientation fluctuations within the motifs being neglected.

For specificity, if we assume two atoms per basis, we may then arrive at the following modification of the two-body potential using the arguments outlined above:

$$\Psi_2(|\mathbf{r}_{ij}|) = V_2\left(\frac{\sigma}{|\mathbf{r}_{ij}|}\right)^{12} \times (1 + \alpha \sin^2 4(\theta_{ij} - \psi)), \tag{12}$$

where the anisotropy parameter α has a fixed value at constant T and P. On the other hand, the three-body potential may be taken to be the same as in equation (5). Setting $\gamma = 1+\alpha$, we see that γ is always positive. All angles are measured with respect to the [01] axes of the undistorted square lattice. The angle ψ represents the orientation of the basis and $\theta_{ij} = \sin^{-1}(x_{ij}/|\mathbf{r}_{ij}|)$; see figure 10. The total energy is a function of ψ, so uniform rotations of the basis with respect to the crystal axes cost energy (optical mode) while simultaneous rotation of the basis together with the crystal axes is a symmetry of the Hamiltonian.

Using the modified two-body potential (equation (12)), we compute the energy as a function of ϵ as in section 3. For fixed α, the total energy minimized with respect to ψ and ϵ leads to $\psi = 0$ (independent of ϵ). As before there are three minima in ϵ, one at $\epsilon = 0$ (corresponding to a square) and the other two corresponding to rhombi with $|\epsilon|$ being *smaller* than the value for the perfect triangular lattice $\sim$0.28 (figure 10). The jump in the value of the shear strain ϵ across the structural transition is therefore smaller than that obtained in section 3.

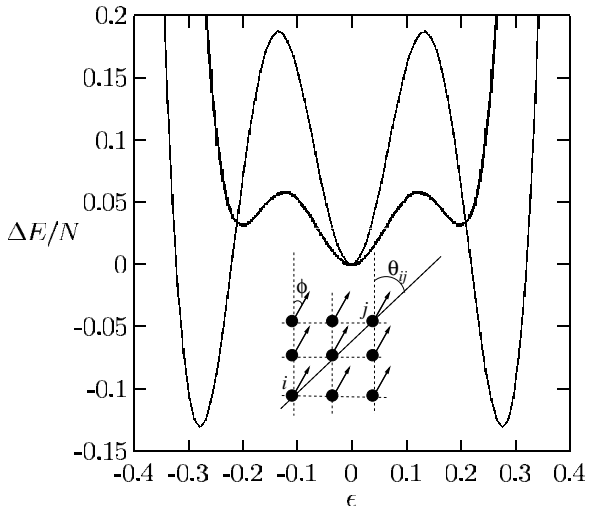

Figure 10. The energy difference $\Delta E/N$ for two values of the anisotropy parameter $\alpha = 0$ and 1 for $V_3 = 1$ and $\rho = 1.1$. Note that the energy minima for $\epsilon \neq 0$ shift to lower values of ϵ as α increases. Inset: the meanings of the angles θ_{ij} and ϕ used in the text. While θ_{ij} is the angle of the position vector $\mathbf{r}_{ij}$ between the molecules i and j measured with respect to the crystal axis {01} in the reference square lattice, ϕ is the orientation of the basis molecule measured with respect to the same axis.

Moreover, we find that this jump in ϵ goes to zero and the region over which the square phase is metastable shrinks and disappears as $V_3 \to 0$, thus indicating a *continuous transition* at a tricritical point. One expects, therefore, that for real systems fluctuation effects near the T–O transition would be more pronounced. This fact is actually borne out by experiments [4, 5].

The zero- and finite temperature phase diagrams are shown in figure 11. The zero-temperature phase diagram clearly shows the location of the tricritical point where the jump in the order parameter vanishes. The effect of finite temperatures is addressed easily within a cell model approximation. The calculation may be carried out along the lines outlined in the last section. Once again we see that the Helmholtz free energy can be written as a power series expansion in ϵ. The results of the calculation are expected to be accurate at low temperatures if the anisotropy is not too large. For larger anisotropies the effect of (tri)critical fluctuations may alter the results for our simple mean-field estimates. Our result shows that the square lattice now becomes stable over a much larger range of V_3 than in the isotropic case. The region of metastability of the square lattice however decreases and the first-order transition is weakened.

6. Nucleation dynamics: selection of ferrite or twinned microstructure

We have discussed, in great detail, the equilibrium phase diagram of a model solid exhibiting a square to triangle transition, including a generalization of the model to a nontrivial basis. Since the primary motivation of our study is to provide a model system for studying the dynamics of nucleation following a quench from one solid phase to another, we would like to end this paper with a short discussion on solid state nucleation dynamics and the kinds of microstructures produced as a result. We shall see that the results obtained are consistent with the phenomenology of real solids. In addition, we find that microstructure selection is intimately linked to the nature of the dynamics of individual particles. Reference [3] contains a detailed account of the nucleation dynamics in this model.

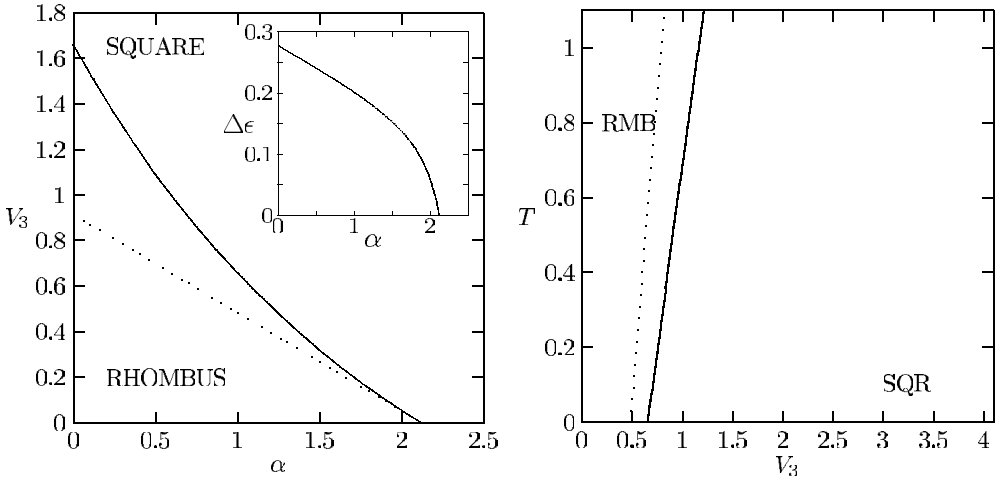

Figure 11. Left: the zero-temperature phase diagram in the V_3–α plane for $\rho = 1.1$. The dashed line marks the limit of metastability of the square phase. Note that for $V_3 = 0$, reducing α produces a second-order transition with a tricritical point at $\alpha_{tc} = 2.24$. The inset shows the jump in the order parameter $\Delta\epsilon$ across the square–rhombus phase boundary as a function of the anisotropy α. Right: the phase diagram in the V_3–T plane for $\alpha = 1$ and $\rho = 1.1$. The dashed line marks the limit of metastability of the square phase. Note that in real systems α depends on T so, in general, any quench traverses a trajectory in the parameter space T–α–V_3 and the first-order line may end in a non-zero-temperature tricritical point.

Consider the MD phase diagram shown in figure 9. Starting from the equilibrium square phase, we may 'quench' into the triangular phase by either changing T or V_3 or both. Experimentally, there are two common protocols—for engineering applications one uses a 'continuous cooling curve' (CCC) [2], where the temperature is reduced at a constant rate across the transition; however, a more instructive protocol is the 'quench-and-hold' one, where the sample is first instantaneously *quenched* to a given temperature T_f and then *held*, so that the sample evolves to its final microstructure at T_f. This procedure is used to map out the 'time–temperature transformation' curves. The quench changes the temperature dependent interaction parameters controlling the structural transition. In our model, the latter transformation protocol can be conveniently carried out by changing V_3 while holding the temperature T fixed.

Interaction parameters such as V_3 may also be tuned experimentally, by changing external fields, such as pressure, electric field or light, which couple to the faster electronic degrees of freedom, thereby affecting the potentials. In the case of colloidal crystals held between glass plates, the crystal structure may be manipulated by external modulating potentials produced by crossed laser beams [28].

Note that in order to follow the dynamics over a significant timescale, we work with much larger system sizes, typically 110×110, than in the equilibrium study (section 4.2).

Consider two typical constant temperature transformation protocols—one at high temperatures and one at low—starting from the equilibrium square and quenching into the region where the square phase is metastable. Following either transformation protocol, the product phase is formed by a process of nucleation and growth as can be seen by following the time dependence of the order parameter $\langle\Omega\rangle \equiv N^{-1}\sum_i \Omega_i = N^{-1}\sum_i (\Omega_0)^{-1}\sum_{jk}\langle\sin^2(4\theta_{ijk})\rangle$. This order parameter has been constructed to take values 0 (1) in the square (triangular) phases respectively (angular brackets denote ensemble averages)

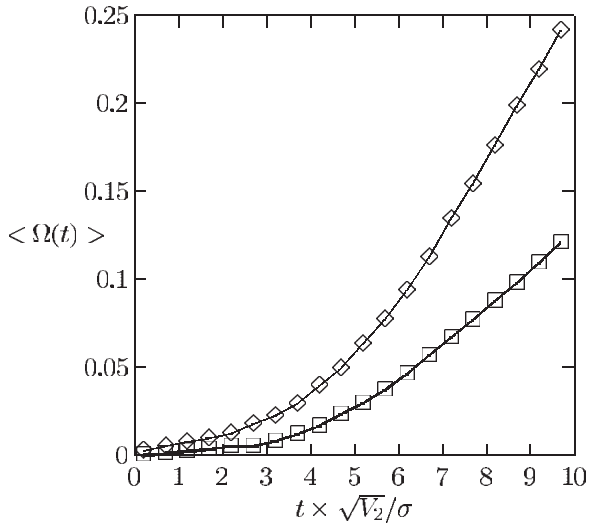

Figure 12. The growth of the order parameter Ω as a function of $t/\tau \equiv t \times \sqrt{V_2}/\sigma$, showing typical nucleation and growth following the high temperature ($\diamond$) and low temperature ($\square$) transformations. The local order parameter Ω_i has been mapped onto a binary representation such that above 90%, we set $\Omega_i = 1$; else, 0. The data have been averaged over the 100 initial conditions for the high temperature and 30 initial conditions for the low temperature quenches. In addition, at each time we have averaged over a small time window. The curves are a guide to the eye.

and is therefore a convenient measure of the amount of 'triangleness' of the region. Figure 12 shows a typical nucleation profile, with an initial 'wait' phase followed by a sharp rise.

The nucleation following the high temperature protocol is *homogeneous*, needing only thermal fluctuations to destabilize the square phase. On the other hand, the nucleation following the low temperature protocol is *heterogeneous*, needing to be promoted by at least a single defect (vacancy) seeded initially into the system by removing a single particle from our 110×110 system, which creates enough strain in the neighbourhood to promote nucleation.

As before, to make contact with continuum physics, we define the coarse grained dynamical nonlinear elastic strain $\epsilon_{ij}(\mathbf{r}, t)$ via instantaneous displacements $\mathbf{u}(\mathbf{r}, t)$ of the particles from the ideal square lattice.

An MD snapshot following the high temperature protocol shows the growth of an 'isotropic' nucleus (figure 13; since this is a snapshot, the nucleus does not appear isotropic; however, when we average over initial conditions and a time and space window, isotropy is restored). Following the collective motion of particles, we find that their trajectories are diffusive and uncorrelated (recall that the microscopic particle dynamics is given by Newton's laws). The critical nucleus is untwinned; the particles within the nucleus have local triangular order as is clear from the values of the local order parameter Ω_i (figure 13). Multiple nucleation events lead to growing nuclei which eventually coalesce to form a polycrystalline triangular solid. Subsequently grain boundaries reorient to form a homogeneous triangular phase (ferrite).

In contrast, an MD snapshot following the low temperature protocol (figure 14) shows a highly anisotropic nucleus (the anisotropy persists on averaging). The collective motion of particles is non-diffusive and highly correlated, producing a 'military' motion characteristic of martensites. The critical nucleus is found to have a twinned structure. In order to show this, figure 14 displays the shear strain ϵ_{xy} measured at fixed time. The inset shows the same profile when integrated over y; the change in sign of ϵ_{xy} marks the position of the twin interface which sharpens with the march of time. Converting to real units, the size of our system

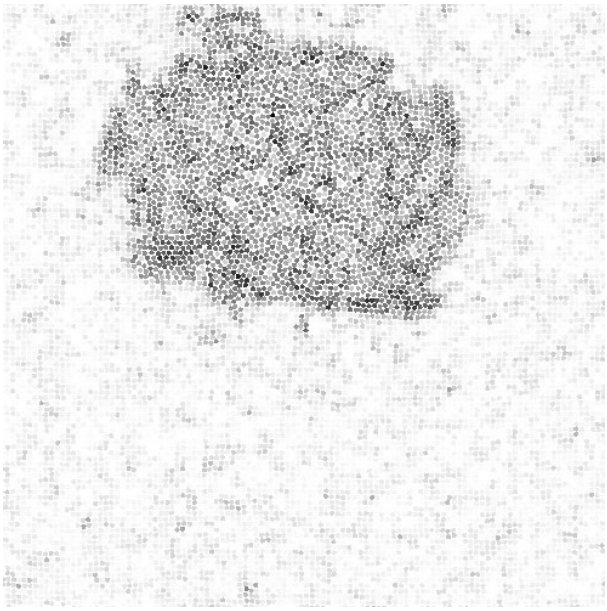

Figure 13. A typical MD snapshot following a transformation at high temperature ($T = 1.1$) showing an isotropic nucleus consisting of particles with local triangular order (black) in a matrix of the square lattice (white). The system size is 12 099 particles and the greyscale goes from $\Omega_i = 0$ (white) to $\Omega_i = 1$ (black).

is approximately 100 Å $\times$ 100 Å. To see multiple twin domain patterns as seen in optical micrographs of real martensites, we need to go to system sizes much larger than this.

Before ending this section, we would like to emphasize the following points. Our model solid shares some of the important equilibrium and dynamical features of 'real' solids, while allowing us to explore a variety of equilibrium and dynamical regimes by simply tuning parameters of the potential and temperature. As we have seen, the same microscopic dynamics for the particles (Newton's laws) gives rise to two distinct dynamical regimes:

(i) At high temperatures, the collective motion of particles is diffusive and the critical nucleus is untwinned and grows isotropically into the equilibrium triangular phase.
(ii) At low temperatures, the collective motion of particles is non-diffusive and coordinated, giving rise to a critical nucleus which is twinned and highly anisotropic. The solid is arrested in a long lived metastable martensite phase.

These dynamical issues have been explored in greater detail in [3]. Note that we have studied the dynamics of solid state transformations for the isotropic two-body potential ($\alpha = 0$). An extension of this study to the case when the two-body potential is anisotropic will appear elsewhere.

7. Conclusion

In this paper we have described a model system which is designed to undergo a square to rhombus transition in two dimensions. We believe that our study will be useful in two ways. On the one hand, it may be used as a simple simulational model for the T–O transition in real materials which often consists of a large number of individual atomic species, making it difficult to study using *ab initio* methods. For this purpose, the parameters V_3 and α have to be

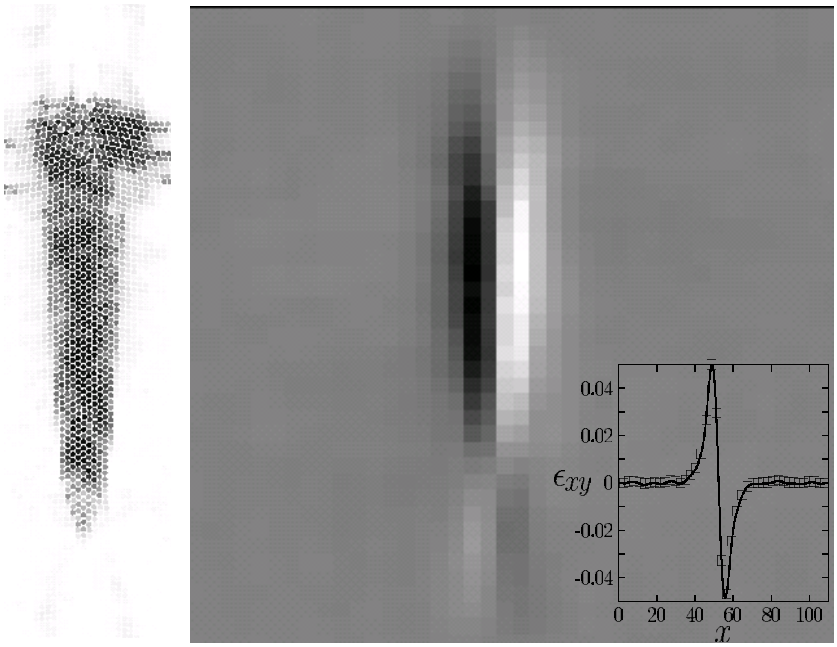

Figure 14. Left: a typical MD snapshot following a transformation at low temperature ($T = 0.1$) showing a highly anisotropic nucleus consisting of particles with local triangular order (black) in a matrix of the square lattice (white). The system size is 12099 particles and the greyscale goes from $\Omega_i = 0$ (white) to $\Omega_i = 1$ (black). Note that the nucleus is twinned. Right: the instantaneous strain ϵ_{xy} profile at $t/\tau = 3$ clearly showing that the growing nucleus is twinned (as the shades go from white to black, the local strain ϵ_{xy} goes from negative to positive values with grey being zero). The inset shows ϵ_{xy} averaged over the vertical direction (the line is a guide to the eye). At these times the strain values fall sharply from a maximum value of 0.05 to a minimum of -0.05 across a twin interface. At later times the absolute values of the maximum and minimum increase and the interface sharpens.

'fitted' to observed properties of the particular realistic system. The effect of defects such as vacancies and dislocations on the equilibrium structural transition of the solid is easily studied within our mesoscopic approach. On the other hand, we could use this system to study, in general, the dynamical pathways of a simple first-order solid state phase transition involving a structural transition. It is this context that we would like to emphasize. We have demonstrated explicitly that our model solid is indeed a good test bed for studying the dynamics of solid state transformations. We have shown that the nature of the transformation protocol (or quench) determines the dynamics of nucleation and the eventual microstructure of the solid. What is the underlying reason for obtaining these different dynamical regimes? These issues and the interplay between the mobility of defects and the dynamics of the order parameter deserve a serious and detailed analysis [3] far exceeding the scope of this paper. In future, we hope to use this model system to obtain microscopically detailed information about the statics and dynamics of solid–solid interfaces.

Acknowledgments

We thank A Sengupta, S Sastry, G Baskaran and especially H K D H Bhadeshia, for useful discussions, and D Chaudhuri, for carefully proofreading the manuscript. We thank the

organizers and participants of the school on 'Mathematical Developments in Solid Mechanics and Materials Science', at The Isaac Newton Institute for Mathematical Sciences, Cambridge (1999), for hospitality and useful discussions. MR thanks the Department of Science and Technology (DST) for a Swarnajayanthi grant. SS acknowledges the Alexander von Humboldt foundation and DST grant SP/S2/M-20/2001 for financial support.

Appendix

In general, evaluation of three-body energies requires sums over all possible triplets which for a system of reasonable size is prohibitively expensive. The particular form for the three-body potential used by us is, however, special and can be evaluated without keeping track of triplets. We illustrate below how this may be done for our system [12, 29] and derive an explicit expression for the energy.

The three-body part of the energy (see equation (1)) is given by

$$\begin{aligned} E_3 &= \tfrac{1}{6}\sum_{i\neq j\neq k}\Psi_3(\mathbf{r}_{ij},\mathbf{r}_{jk},\mathbf{r}_{ki}) \\ &= \frac{1}{2}\sum_{i\neq j\neq k}\frac{V_3}{4}f_{ij}\sin^2(4\theta_i)f_{ik} \\ &= \sum_{i\neq j\neq k}2(\sin^2\theta_i\cos^2\theta_i - 4\sin^4\theta_i\cos^4\theta_i)f_{ij}f_{ik}. \end{aligned} \tag{13}$$

Now define $\tilde{x}_{ij} = x_{ij}/r_{ij}$ and $\tilde{y}_{ij} = y_{ij}/r_{ij}$, so that $\sin\theta_i = \tilde{x}_{ik}\tilde{y}_{ij} - \tilde{x}_{ij}\tilde{y}_{ik}$ and $\cos\theta_i = \tilde{x}_{ik}\tilde{y}_{ij} + \tilde{x}_{ij}\tilde{y}_{ik}$. Using the above definitions and the quantities

$$\begin{aligned} g_{ij}(1) &= \tilde{x}_{ij}^2\tilde{y}_{ij}^2 f_{ij}, \\ g_{ij}(2) &= \tilde{x}_{ij}^2\tilde{y}_{ij}^2(\tilde{x}_{ij}^2 - \tilde{y}_{ij}^2) f_{ij}, \\ g_{ij}(3) &= \tilde{x}_{ij}^4\tilde{y}_{ij}^4 f_{ij}, \\ g_{ij}(4) &= \tilde{x}_{ij}^2\tilde{y}_{ij}^2(\tilde{x}_{ij}^2 - \tilde{y}_{ij}^2)^2 f_{ij}, \\ g_{ij}(5) &= \tilde{x}_{ij}^3\tilde{y}_{ij}^3(\tilde{x}_{ij}^2 - \tilde{y}_{ij}^2) f_{ij}, \end{aligned} \tag{14}$$

we get $E_3 = V_3\sum_i S_i$ with

$$\begin{aligned} S_i = 4[G_i(1)F_i - 4G_i(1)^2 - G_i(2)^2] - 16 \\ \times\{G_i(3)F_i + 32G_i(3)^2 + 2G_i(4)^2 + G_i(1)^2 \\ - 16G_i(3)G_i(1) - 4G_i(5)G_i(2) + 16G_i(5)^2\} \end{aligned} \tag{15}$$

and $G_i(n) = \sum_{j\neq i} g_{ij}(n)$ and $F_i = \sum_{j\neq i} f_{ij}$. The three-body forces can be obtained by taking derivatives of E_3 which can be cast into a similar form.

References

[1] Khachaturyan A G 1983 *The Theory of Structural Transformations in Solids* (New York: Wiley)
Olson G B and Owen W S (ed) 1992 *Martensite* (Metals Park, OH: American Society of Metals)
[2] *Metals Handbook* 1973 (Metals Park, OH: American Society of Metals)
[3] Rao M and Sengupta S 2003 *Phys. Rev. Lett.* **91** 045502
[4] Jacobs A E 1985 *Phys. Rev.* B **31** 5984
Kartha S, Castán T, Krumhansl J A and Sethna J P 1991 *Phys. Rev. Lett.* **67** 3630
Kartha S, Krumhansl J A, Sethna J P and Wickham L K 1995 *Phys. Rev.* B **52** 803
Onuki A 1999 *J. Phys. Soc. Japan* **68** 5
Shenoy S R, Lookman T, Saxena A and Bishop A R 1999 *Phys. Rev.* B **60** 12537

[5] King A H and Zhu Y 1993 *Phil. Mag.* A **67** 1037
Zhu Y, Suenaga M and Tafto J 1993 *Phil. Mag.* A **67** 1057
Chu C 1993 *PhD Thesis* Univ. Minnesota
[6] Sankararaman S and Shankar R 2003 *Phys. Rev.* B **67** 245102
Rao M, Sengupta S and Shankar R 1997 *Phys. Rev. Lett.* **79** 3998
[7] Falk F 1983 *Z. Phys.* B **51** 177
Barsch G R and Krumhansl J A 1984 *Phys. Rev. Lett.* **53** 1069
[8] Semenovskaya S and Khachaturyan A G 1991 *Phys. Rev. Lett.* **67** 2223
Semenovskaya S and Khachaturyan A G 1992 *Phys. Rev.* B **46** 6511
Semenovskaya S, Zhu Y, Suenaga M and Khachaturyan A G 1993 *Phys. Rev.* B **47** 12182
[9] Rao M and Sengupta S 1997 *Phys. Rev. Lett.* **78** 2168
Rao M and Sengupta S 1999 *Curr. Sci.* **77** 382
[10] Sengupta S, Nielaba P, Rao M and Binder K 2000 *Phys. Rev.* E **61** 1072
Sengupta S, Nielaba P and Binder K 2000 *Phys. Rev.* E **61** 6294
[11] Becquart C S, Clapp P C and Rifkin J A 1993 *Phys. Rev.* B **48** 6
Meyer R and Entel P 1997 *LANL Preprint* cond-mat/9706248
Daw M S and Baskes M I 1983 *Phys. Rev. Lett.* **50** 1285
Daw M S and Baskes M I 1984 *Phys. Rev.* B **29** 6443
[12] Weber T A and Stillinger F H 1993 *Phys. Rev.* E **48** 4351
[13] Squire D R, Holt A C and Hoover W G 1969 *Physica* **42** 388
[14] Hoover W G, Ashurst W T and Grover R 1972 *J. Chem. Phys.* **57** 1259
Hoover W G, Hoover N E and Hanson K 1979 *J. Chem. Phys.* **70** 1837
Hoover W G and Ree F H 1968 *J. Chem. Phys.* **49** 3609
[15] Frenkel D and Smit B 1996 *Understanding Molecular Simulations* (San Diego, CA: Academic)
[16] Chaikin P M and Lubensky T C 1995 *Principles of Condensed Matter Physics* (Cambridge: Cambridge University Press)
[17] Born M and Huang K 1998 *Dynamical Theory of Crystal Lattices* (Oxford: Oxford University Press)
[18] Ramakrishnan T V and Yussouff M 1979 *Phys. Rev.* B **19** 2775
[19] Hansen J-P and McDonald I R 1986 *Theory of Simple Liquids* (London: Academic)
[20] See for e.g. Denton A R and Ashcroft N W 1989 *Phys. Rev.* A **39** 426
[21] For reviews of density wave theory see e.g.
Tareyeva E and Ryzhov V 1997 *LANL Preprint* cond-mat/9712265
Löwen H 1994 *Phys. Rep.* **237** 249
Hansen J-P, Levesque D and Zinn-Justin J (ed) 1991 *Liquids, Freezing and Glass Transition (Les Houches)* (Amsterdam: North-Holland)
[22] Denton A R, Kahl G and Hafner J 1999 *J. Non-Cryst. Solids* **15** 250
[23] Rosenfeld Y 1990 *Phys. Rev.* A **42** 5978
[24] A similar situation exists for the body centered cubic lattice in three dimensions. Second-order contributions always prefer a close-packed face centered cubic structure and in order to discuss the relative stability of these two lattices three body correlations have to be invoked ;
Sengupta S 1991 *PhD Thesis* Indian Institute of Science, Bangalore
For an application to the system of charge stabilized colloids, see
Sengupta S and Sood A K 1991 *Phys. Rev.* A **44** 1233
Choudhury N and Ghosh S K 1995 *Phys. Rev.* E **51** 4503
[25] Landau L D and Lifshitz E M 1986 *Theory of Elasticity* 3rd edn (Oxford: Pergamon)
[26] Scott J F 1974 *Rev. Mod. Phys.* **46** 83
[27] Such a treatment has been commonly used in the study of phase transitions in liquid crystals using density wave theory, see for e.g.
Singh Y 1984 *Phys. Rev.* A **30** 583
Mahato M C, Lakshmi M R, Pandit R and Krishnamurthy H R 1988 *Phys. Rev.* A **38** 1049
[28] Yethiraj A, Wouterse A, Groh B and van Blaaderen A 2004 *Phys. Rev. Lett.* **92** 058301
See also articles in Arora A K and Tata B V R (ed) 1996 *Ordering and Phase Transitions in Charged Colloids* (New York: VCH)
[29] Biswas R and Hamann D R 1987 *Phys. Rev.* B **36** 6434